Mechanical Tunability of an Ultranarrow Spectral Feature of a Rare-Earth-Doped Crystal via Uniaxial Stress

N. Galland, N. Lučíc, B. Fang, S. Zhang, R. Le Targat, A. Ferrier, P. Goldner, S. Seidelin, Y. Le Coq

Mechanical Tunability of an Ultranarrow Spectral Feature of a Rare-Earth-Doped Crystal via Uniaxial Stress

N. Galland,[1,2] N. Lučić,[2] B. Fang,[2] S. Zhang,[2] R. Le Targat,[2] A. Ferrier,[3,4] P. Goldner,[3] S. Seidelin,[1,5,*] and Y. Le Coq[2]

[1] *Université Grenoble Alpes, CNRS, Grenoble INP and Institut Néel, 38000 Grenoble, France*
[2] *LNE-SYRTE, Observatoire de Paris, Université PSL, CNRS, Sorbonne Université, Paris, France*
[3] *Chimie ParisTech, Université PSL, CNRS, Institut de Recherche de Chimie Paris, 75005 Paris, France*
[4] *Sorbonne Université, Faculté des Sciences et Ingénierie, UFR 933, 75005 Paris, France*
[5] *Institut Universitaire de France, 103 Boulevard Saint-Michel, F-75005 Paris, France*

(Received 28 October 2019; revised manuscript received 16 March 2020; accepted 23 March 2020; published 8 April 2020)

Rare-earth-doped crystals have numerous applications ranging from frequency metrology to quantum information processing. To fully benefit from their exceptional coherence properties, the effect of mechanical strain on the energy levels of the dopants—whether it is a resource or perturbation—needs to be considered. We demonstrate that by applying uniaxial stress to a rare-earth-doped crystal containing a spectral hole, we can shift the hole by a controlled amount that is larger than the width of the hole. We deduce the sensitivity of Eu^{3+} ions in an Y_2SiO_5 matrix as a function of the crystal site and the crystalline axis along which the stress is applied.

DOI: 10.1103/PhysRevApplied.13.044022

I. INTRODUCTION

Rare-earth ions embedded in a crystalline matrix, at cryogenic temperatures, exhibit optical transitions with excellent coherence properties [1,2] and offer the ease of use of solid-state materials. Such properties can be used in, for example, classical [3,4] and quantum [5–9] information processing schemes, quantum optical memories [10–12], quantum probes of photonic effects [13], and in ultrahigh-precision laser stabilization and spectroscopy [14–17]. In these materials, randomly distributed perturbations from the local matrix result in a broad inhomogeneous profile of the ion absorption spectrum, but spectral-hole-burning (SHB) techniques can be used to realize narrow spectral features with a resolution that is only limited by the individual ion dopants. Moreover, as the spectral properties of the individual ions are sensitive to the surrounding crystalline matrix, external stress applied to the crystal in the elastic regime, in which the deformation is proportional to the applied stress and no irreversible modification or deformation of the crystal occurs, will displace in frequency a previously imprinted spectral hole. This provides an interesting resource for tuning spectral holes reversibly, in addition to probing stress fields in a spatially resolved manner. Other applications of stress sensitivity can be found in the field of quantum optomechanics [18], where the vibrations of a mechanical resonator modulate the energy levels of quantum two-level system emitters embedded in the resonator material itself, as observed experimentally in resonators containing quantum dots [19] or nitrogen-vacancy (N-V) centers [20–22] and proposed theoretically for rare-earth-ion-doped resonators [23,24].

II. PHYSICAL SYSTEM AND EXPERIMENTAL SETUP

In this work, we focus on Eu^{3+} ions in a Y_2SiO_5 host matrix (Eu:YSO) at a temperature of 3.15 K, as this material exhibits one of the narrowest optical transitions among solid-state emitters. We exploit the 580-nm optical transition $^7F_0 \rightarrow {}^5D_0$, which possesses near lifetime limited coherence times in the millisecond range [25,26]. The YSO crystal has two nonequivalent locations within the unit cell where Eu^{3+} can substitute for Y^{3+}, referred to as sites 1 and 2 (vacuum wavelengths of 580.04 and 580.21 nm, respectively). We use the SHB technique to benefit from the narrow homogeneous line width and at the same time the large signal-to-noise ratio coming from working with an ensemble of ions. In our system, the spectral holes are formed by resonant optical excitation and decay of the ions into other long-lived (several hours) dark states corresponding to other hyperfine levels within the electronic-ground-state manifold [27]. Subsequent scanning of the frequency of a weak optical field across the hole will allow observation of the structure.

The experimental setup is shown in Fig. 1. The laser system is based on two fiber-coupled extended-cavity cw

*signe.seidelin@neel.cnrs.fr

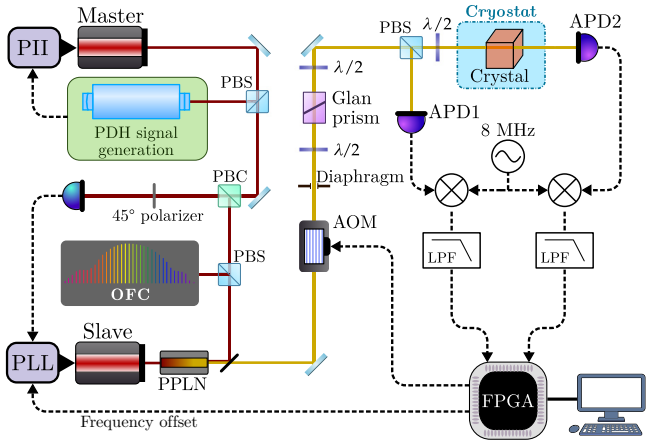

FIG. 1. The schematics of the experimental setup used for measuring the strain sensitivity. The following abbreviations are used: ML, master laser; SL, slave laser; PDH, Pound-Drever-Hall; APD1 and APD2, avalanche photodetectors 1 and 2; PLL, phase-lock loop; PII, proportional double-integrator corrector; AOM, acousto-optical modulator; FPGA, field-programmable gate array; LPF, low-pass filter; PPLN, periodically poled lithium niobate; OFC, optical frequency comb; PBS (PBC) polarizing beam splitter (polarizing beam combiner)—the same device with different functions.

diode lasers (ECDL), referred to as the master and slave laser, operating at 1160 nm and delivering 65 mW each. The master laser is frequency locked (locking bandwidth around 800 kHz) by the Pound-Drever-Hall (PDH) method to a commercial reference cavity (finesse approximately 300.000). It exhibits a fractional frequency instability below 10^{-14} for time constants of 1–100 s, for radiation with line width of a few hertz. The slave laser is offset phase locked [28] to the master laser (with a lock bandwidth of typically 1 MHz) in order to benefit from the spectral stability of the master laser [16,17]. The slave-laser frequency and phase are set, in the phase-lock loop, by adjusting the current of the diode laser, with an additional slow action on a piezoelectric actuator that can change the laser external-cavity length. The optical frequency is then doubled in a periodically poled lithium-niobate (PPLN) waveguide with free space output to produce 4.5 mW of radiation near 580 nm.

Further control of the 580-nm laser field generated by the slave laser is provided by an acousto-optic modulator (AOM) used in a double-pass configuration and driven by an rf signal generated by a computer-controlled field-programmable gate array (FPGA). By choosing accordingly the reference Fabry-Perot-cavity mode onto which the master laser is frequency locked (the free spectral range of the cavity is near 1.5 GHz) and the frequency difference between the master and slave lasers (in practice, the frequency offset of 850 MHz is used throughout the work described in this paper), we ensure that the frequency of the slave laser at 580 nm is positioned near the center of the Eu:YSO crystal absorption profile (for either site 1 or site 2). The 580-nm light beam from the slave laser then passes through a $\lambda/2$ wave plate and a Glan polarizer for tunable attenuation and lenses are used to adjust the beam diameter to 6 mm, followed by a tunable aperture that allows the beam size to be restricted further. A second $\lambda/2$ wave plate followed by a second polarizing beam splitter then allows the beam to be split into two parts (with adjustable relative intensities), one part sent directly to a silicon avalanche photodiode (APD1 in Fig. 1) while the other passes through the crystal, after polarization tuning via a final $\lambda/2$ wave plate, before being sent to a second avalanche photodiode (APD2). This last wave plate allows tuning of the polarization (parallel to the D_1 axis) for optimum absorption in the crystal [29].

When burning a spectral hole, the first wave plate is rotated such that the optical intensity is at a maximum on the crystal and a single tone is applied to the AOM, typically producing 70 μW/cm^2 during 0.5 s. When probing the hole, the AOM is driven with an appropriate rf waveform so as to produce two optical tones [30], separated by 800 kHz, jointly frequency scanned at 100 kHz/s, one of them in the vicinity of the spectral hole. The first wave plate is also rotated to decrease the optical intensity (400 nW/cm^2 in each mode). The corresponding detected beat notes on the APDs (800 kHz) are up-converted to 8.8 MHz (by mixing with an 8-MHz signal), digitized, digitally down-converted to the base band, and streamed to a computer, which filters them in a 15-kHz bandwidth and extracts the transmission of the crystal from the comparison (division) between the amplitude of the signals from APD1 and APD2. This particular data processing allows minimization of the excess low-frequency noise of photodiodes, amplifiers, and analog-to-digital converters.

We use a commercial closed-cooling-cycle cryostat (OptiDry from MyCryoFirm) to maintain the crystal at 3.15 K, with a passive vibration-isolation stage between the cooler and the science chamber and a commercial active-vibration-canceling platform supporting the science chamber itself. Due to this combination of passive and active cancellation, we observe that the spectral hole is unaffected by the mechanical vibration induced by the cooling cycle of the cryostat, i.e., the spectral hole is identical whenever in the 0.7-s-period cooling cycle it is monitored [17]. The science chamber is composed of a thermally stabilized 3.15-K copper plate and an enclosing shield, with 25-mm-diameter windows for optical access.

The Eu:YSO crystal is grown by the Czochralski process, with a resulting 0.1-at.% europium doping. After x-ray orientation, it is cut into a $8 \times 8 \times 4$ mm^3 cuboid, such that the optical beam can propagate along the crystallographic b axis, and the two other facets are oriented along the principal dielectric axes D_1 and D_2, parallel to which we wish to apply mechanical stress. The two largest facets of the crystal, perpendicular to the b axis, are polished

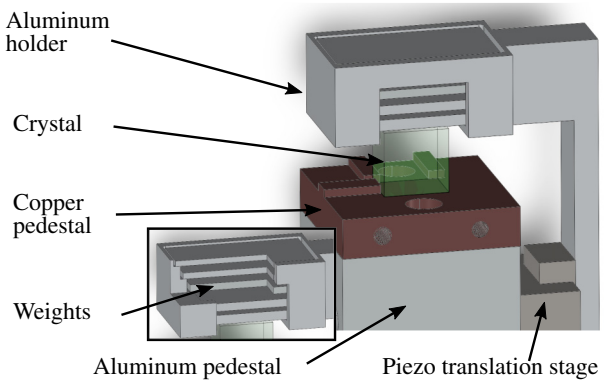

FIG. 2. The schematics of the mount and the motorized piezo stage, with which we can deposit (or remove) a given number of weights on the top of the crystal inside the cryostat, allowing several different values of a calibrated stress to be applied to the crystal. The inset shows an enlargement of the inside of the staircaselike structure.

for optical-beam propagation and set with a small relative angle (2°) to prevent intrusive Fabry-Perot-cavity buildup. In order to apply the stress parallel to the D_1 axis, the crystal is oriented such that this axis is in the vertical direction. We then rotate the crystal 90° to perform the measurements with a stress applied parallel to the D_2 axis. The crystal is mounted in the science chamber inside the cryostat, on a specially designed pedestal (see Fig. 2).

III. CREATION OF A HOMOGENEOUS STRESS FIELD ACROSS THE CRYSTAL

The strain sensitivity of the Eu^{3+} ions in the YSO matrix when applying an isotropic pressure by changing the helium gas pressure inside a cryostat has been measured by another group [15]. However, for all applications discussed above, the uniaxial strain sensitivity is needed, which requires the application of a calibrated force inside the cryostat in a single given direction. To achieve this, we use a staircaselike structure (see inset in Fig. 2) the vertical position of which is controlled by a motorized platform situated inside the cryostat, providing a simple way of placing a variable number of objects on the top of the crystal. Once placed on the crystal, the objects (metal plates) are physically separated from the mount (and the remaining objects still on the mount). The masses of the objects and the size of the crystal are measured prior to insertion in the cryostat in order to provide a well-calibrated force. We start the sequence by burning a spectral hole with no weights on the crystal and we then add them one by one, each time recording the profile of the spectral hole. The beam diameter for probing is approximately 2 mm, which is small compared to the polished facet of the crystal. For verification, the measurements are also repeated by burning the spectral hole with all weights on the top of the crystal and then removing them one by one, recording the spectra (corresponding to negative stress). The measurements are also repeated in several different locations of the crystal, to ensure that the strain field is nearly homogeneous. The impact of the scanning on the long-lived persistent spectral features is negligible during the typical time constant of the experiment (a few minutes for five or six scans).

To create a sufficiently homogeneous strain field, we use a three-axis piezo translation stage, two of these axes being used for fine centering of the weights on the crystal and the last, vertical, axis being used for operating the staircase deposition structure. As the energy transitions in Eu^{3+} are not only sensitive to mechanical strain but also electric fields [31–33], special care is required to eliminate uncontrolled residual electrical field and charges. In particular, the motorized platform and crystal are both surrounded by independently grounded aluminum shields and a cover. Finally, for the weights to produce homogeneous strain in the crystal, we find it necessary to add a layer (approximately 1 mm thick) of powderized YSO that does not contain europium ions (typical grain size in the micrometer range) on the top and bottom of the crystal. We further note that the silver lacquer commonly used in cryogenics for ensuring good thermal contact between the crystal and the cold finger produces comparatively large unpredictable stress on the crystal and has to be avoided. Thermalization of the crystal relies solely on radiation and heat exchange through the top and bottom powder layers, and a typical waiting time of 5 min is used to reach steady state when necessary—in particular, after operation of the translation stages for relatively large (more than 5-mm) excursions (which are found to momentarily perturb the temperature stability). The frequency drift of the cavity is continuously monitored using the beat note of our laser with a frequency comb (also shown in Fig. 1) but the drift consistently turns out to be negligible.

IV. RESULTS OF MEASUREMENTS OF STRESS-INDUCED FREQUENCY SHIFTS

An example of the displacement of a spectral hole (of an initial width of approximately 4 kHz) consisting of ions occupying crystal site 2 when applying uniaxial stress along the D_1 crystalline axis is shown in Fig. 3(a). In addition to the displacement of the center of the spectral hole, we also observe a broadening of the profile, which is partly due to inhomogeneities on the microscopic level in the different ions' response to applied strain, as observed in other rare-earth-doped systems [34,35], partly due to a residual inhomogeneity in the applied strain.

The measurements are repeated when applying stress along both the D_1 and D_2 crystalline axes and for both crystal sites 1 and 2. In Fig. 3(b), we plot the frequency shift of the center of the spectral hole as a function of the stress applied to the crystal, for the different axes and crystal sites. The largest contribution to the errors stems from

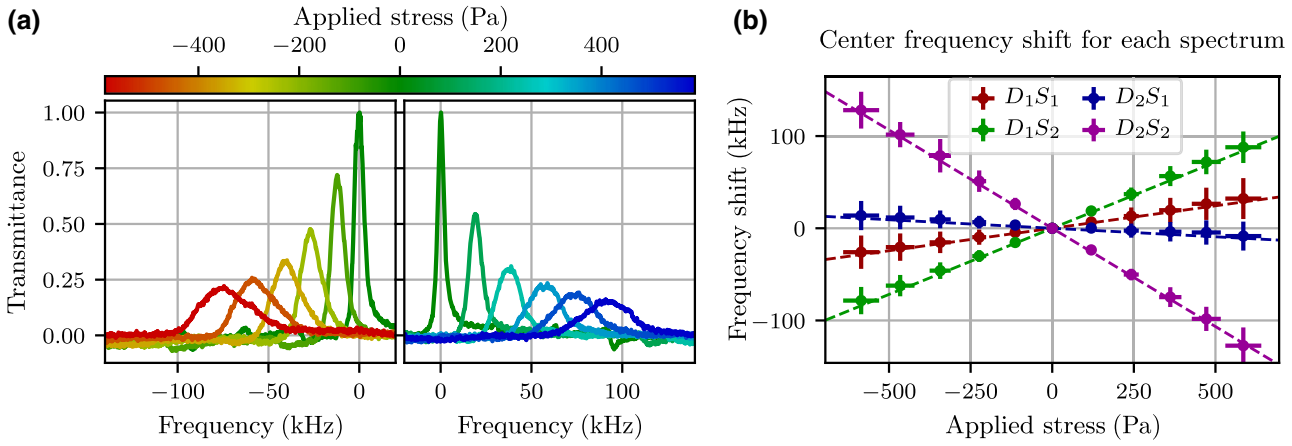

FIG. 3. When stress is applied to the crystal, the profiles of the spectral holes shift in frequency. (a) The behavior of the spectral hole under stress corresponding to crystal site 2, with the stress applied parallel to D_1 (D_1S_2). Positive values of the stress correspond to adding weights one by one following the SHB, whereas negative values correspond to burning the holes with all the weights on the top of the crystal and then removing them one by one. (b) The displacements of the center of the spectral hole for different axes (D_1 and D_2) parallel to which the stress is applied and different crystal sites (S_1 and S_2), with linear fits to the data.

the inhomogeneity in direction and amplitude of the strain. We include this uncertainty by assigning horizontal error bars inferred from measurements of the displacements in different locations in the crystal (the contribution from the uncertainty due to the measurements of the masses of the weights and the crystal size is negligible) and a vertical error bar that reflects the full width at half maximum of the spectral hole.

We observe a systematic tendency of some data points to be marginally above the linear fit in Fig. 3(b). This phenomenon may need further study but a possible explanation is that the operation of the translation stage locally creates a minute increase in temperature (despite the waiting time) at the position of the crystal. As the resonant frequency of the hole is also dependent on the temperature [15], the heating gives rise to a small systematic frequency shift that is positive for both the positive and negative stresses applied and has no or a negligible impact on the final values of the slopes extracted from the linear fits. Finally, we repeat the measurements for spectral holes situated in different parts of the inhomogeneously broadened profile and again obtain stress sensitivities confined to within the error bars. We observe that within the range of the measurement, the central shifts are linear with the applied stress and we extract proportionality coefficients from fits. The weighted average of several data sets provides the final values, shown in Table I, where the stated uncertainty stems from a combination of the square root of the relevant diagonal elements of the covariance matrix terms for each fit and the repeatability of the measurement series.

As described above, these values are obtained by studying the displacement of a spectral hole but the values directly apply to the shifts of the energy levels of the individual europium ions constituting the spectral hole.

V. APPLICATIONS AND OUTLOOK

The measurements performed here are useful for many applications in a variety of research domains. A first such domain is in (quantum or classical) optomechanics, where strain-mediating coupling between a mechanical resonator and an atomlike quantum system allows for probing and acting optically on the mechanical resonator. Other systems potentially suitable for strain-coupled quantum systems, such as N-V and Si-V centers in diamond, tend to exhibit a somewhat higher sensitivity for optical transitions. In particular, maximum sensitivities as high as 1000 Hz/Pa in N-V^- centers [36] and 1800 Hz/Pa in Si-V^- centers [37] have been reported, a factor of 5–10 larger than for the system reported here. However, the sensitivity should be compared to the line width of the corresponding optical transitions, which can be as low as 122 Hz for the considered transition in Eu:YSO [25], whereas the corresponding optical transitions (for the zero-phonon line in bulk material) are 13 MHz in N-V^- [38] and 322 MHz

TABLE I. Strain sensitivities for europium ions in a YSO matrix when stress is applied parallel to either one of the crystalline axes D_1 or D_2 and for crystal site 1 or 2.

Axis	Site	Hz Pa^{-1}	THz per strain
D_1	1	46 ± 17	6.2 ± 2.3
D_1	2	137 ± 16	18 ± 2.2
D_2	1	-19 ± 10	-2.6 ± 1.4
D_2	2	-213 ± 13	-29 ± 1.8

in Si-V^- [39], both already close to their lifetime-limited values. This is at least 5 orders of magnitude larger than for the europium ions considered here. Although, for most physical applications, the sensitivity to stress is the most relevant quantity, in order to compare different systems from a microscopic point of view, the sensitivity per strain is preferably used, which is independent of the stiffness of the crystal. These values, also given in the table, are calculated using a Young's modulus for YSO of 135 GPa. Due to the high Young's modulus in diamond (1220 GPa), on a microscopic level, the strain sensitivity is increased by an additional order of magnitude in these systems. The smaller sensitivity for the rare-earth dopants partly stems from the protection of the $4f$ orbitals (within which the optical transition takes place) by the outer s and p orbitals—the same effect being, in part, the origin of the long coherence times. In the context of strain-coupled nano-optomechanics, the uniaxial strain sensitivity measured in this work should be sufficiently large to provide a direct observation of the quantum features of a mechanical resonator, such as the zero-point motion [23,24].

A second domain in which our measurement may be useful is for the development of highly sensitive accelerometers or relative gravimeters. Utilized in such a context with a test mass of 1 kg and staying well below the elastic limit of YSO (approx. 100 MPa [40]), our $8 \times 8 \times 4$ mm^3 crystal would exhibit a frequency shift of 6.6 MHz per m s^{-2} in the most sensitive site and direction. Assuming shot-noise-limited dispersion-based detection of the position of the spectral hole [16,17] with a typical slope of 0.1 mrad/Hz and with 100 nW of probing power, this corresponds to a sensitivity of 1×10^{-6} rad/$\sqrt{\text{Hz}}$/(660 rad/m s^{-2}) $= 1.4 \times 10^{-9}$ m s^{-2}/$\sqrt{(\text{Hz})}$. This is competitive with all existing commercial technology accelerometers and could hold promise as an interesting application of rare-earth-doped materials.

Last but not least, this measurement is also of strong interest for applications requiring extreme frequency stability of the spectral hole, such as ultrastable cw laser realization for optical atomic clocks [15–17]. The sensitivity coefficients that we measure provide a limit to the level of acceptable residual mechanical vibrations. For instance, obtaining a laser with a relative frequency stability of 10^{-18} at 1 s by locking it to a spectral hole would require (when considering the least sensitive direction and crystal site) a noise level below approximately 10^{-6} m s^{-2}/$\sqrt{(\text{Hz})}$ near 1 Hz frequency, which is likely within reach. In more detail, due to the 1.1 g mass of the $8 \times 8 \times 4$ mm^3 bare crystal that we use here, photoimprinted spectral holes will exhibit a sensitivity to vibration-induced accelerations between 1.5×10^{-11}(m s^{-2})$^{-1}$ and 1.3×10^{-12}(m s^{-2})$^{-1}$, depending on the site and direction considered. This is roughly similar to the sensitivities of high-quality Fabry-Perot-cavity systems (see, e.g., Refs. [41,42]): we emphasize, however, that such systems utilize specially engineered mountings and geometries, based on finite-element simulation and/or symmetric designs, to minimize the vibration sensitivity. On the contrary, in our work we measure properties intrinsic to the material and a strong reduction of the *effective* sensitivity can be predicted by using, similarly, specially designed crystal mounts, in the spirit of that described in Ref. [15] but now based on quantitative knowledge of the material response provided in this paper. Furthermore, Wiener-filter-based active-noise canceling similar to what has been shown for Fabry-Perot-cavity-based systems [43] may be adapted to SHB-crystal-based systems as well, further lowering the effective sensitivity for specific applications.

VI. CONCLUSION

Our demonstration of the mechanical tunability of the frequency of a spectral hole in Eu^{3+}:Y_2SiO_5 at cryogenic temperature, combined with quantitative measurements of the uniaxial stress sensitivity, evidences an important fundamental effect that may be utilized in a large variety of applications ranging from quantum nano-optomechanics to high-precision measurements. Moreover, due to the long lifetime of the spectral features, this tunable quantum hybrid system thus possesses an inherent memory, which is unique among solid-state emitters. The low degree of symmetry of the two nonequivalent substitution sites as well as of the crystal itself makes it extremely challenging to calculate the stress-sensitivity coefficients *ab initio*. Therefore, our measurements are essential in order to predict the relevance and limitations of the many potential applications of this system, in addition to serving as an input for theoretical models. The strain sensitivity of the 580-nm transition in Eu^{3+}:Y_2SiO_5 is a factor of 5–10 times smaller than values measured for optical transitions in other dopants such as N-V and Si-V centers in diamond. However, the homogeneous line width for europium ions can be 5 orders of magnitude narrower than the corresponding optical transition in N-V and Si-V systems, making rare-earth-doped systems interesting candidates for strain-engineered quantum systems that rely on a transition that can be directly addressed optically.

ACKNOWLEDGMENTS

We thank A. C. Bleszynski Jayich, S. Kröll, S. Horvath, T. Chanelière, R. Ahlefeldt, K. Mølmer, J. Sankey, and E. Dupont-Ferrier for useful discussions. The project has been supported by the European Union's Horizon 2020 research and innovation program under Grant Agreement No. 712721 (NanOQTech). It has also received support from the Ville de Paris Emergence Program, the Région Ile de France DIM C'nano and SIRTEQ, the LABEX Cluster of Excellence FIRST-TF (ANR-10-LABX-48-01) within the Program "Investissements d'Avenir" operated by the French National Research Agency (ANR), and the OC18

project (Grant Agreement No. 15SIB03) of the EMPIR program cofinanced by the Participating States and the European Union's Horizon 2020 research and innovation program.

[1] C. W. Thiel, T. Böttger, and R. L. Cone, Rare-earth-doped materials for applications in quantum information storage and signal processing, J. Lumin. **131**, 353 (2011).

[2] M. Rančić, M. P. Hedges, R. L. Ahlefeldt, and M. J. Sellars, Coherence time of over a second in a telecom-compatible quantum memory storage material, Nat. Phys. **14**, 50 (2018).

[3] P. Berger, Y. Attal, M. Schwarz, S. Molin, A. Louchet-Chauvet, T. Chanelière, J.-L. Le Gouët, D. Dolfi, and L. Morvan, RF spectrum analyzer for pulsed signals: Ultra-wide instantaneous bandwidth, high sensitivity, and high time-resolution, J. Lightwave Technol. **34**, 4658 (2016).

[4] C. Venet, M. Bocoum, J.-B. Laudereau, T. Chanelière, F. Ramaz, and A. Louchet-Chauvet, Ultrasound-modulated optical tomography in scattering media: Flux filtering based on persistent spectral hole burning in the optical diagnosis window, Opt. Lett. **43**, 3993 (2018).

[5] M. Nilsson and S. Kröll, Solid state quantum memory using complete absorption and re-emission of photons by tailored and externally controlled inhomogeneous absorption profiles, Opt. Commun. **247**, 393 (2005).

[6] F. Bussières, C. Clausen, A. Tiranov, B. Korzh, V. B. Verma, S. W. Nam, F. Marsili, A. Ferrier, P. Goldner, H. Herrmann, C. Silberhorn, W. Sohler, M. Afzelius, and N. Gisin, Quantum teleportation from a telecom-wavelength photon to a solid-state quantum memory, Nat. Photonics **8**, 775 (2014).

[7] A. Walther, L. Rippe, Y. Yan, J. Karlsson, D. Serrano, A. N. Nilsson, S. Bengtsson, and S. Kröll, High-fidelity readout scheme for rare-earth solid-state quantum computing, Phys. Rev. A **92**, 022319 (2015).

[8] N. Maring, P. Farrera, K. Kutluer, M. Mazzera, G. Heinze, and H. de Riedmatten, Photonic quantum state transfer between a cold atomic gas and a crystal, Nature **551**, 485 (2017).

[9] A. M. Dibos, M. Raha, C. M. Phenicie, and J. D. Thompson, Atomic Source of Single Photons in the Telecom Band, Phys. Rev. Lett. **120**, 243601 (2018).

[10] T. Zhong, J. M. Kindem, J. G. Bartholomew, J. Rochman, I. Craiciu, E. Miyazono, M. Bettinelli, E. Cavalli, V. Verma, S. W. Nam, F. Marsili, M. D. Shaw, A. D. Beyer, and A. Faraon, Nanophotonic rare-earth quantum memory with optically controlled retrieval, Science **357**, 1392 (2017).

[11] C. Laplane, P. Jobez, J. Etesse, N. Gisin, and M. Afzelius, Multimode and Long-Lived Quantum Correlations Between Photons and Spins in a Crystal, Phys. Rev. Lett. **118**, 210501 (2017).

[12] A. Seri, A. Lenhard, D. Rieländer, M. Gündoğan, P. M. Ledingham, M. Mazzera, and H. de Riedmatten, Quantum Correlations between Single Telecom Photons and a Multimode On-Demand Solid-State Quantum Memory, Phys. Rev. X **7**, 021028 (2017).

[13] K. J. Tielrooij, L. Orona, A. Ferrier, M. Badioli, G. Navickaite, S. Coop, S. Nanot, B. Kalinic, T. Cesca, L. Gaudreau, Q. Ma, A. Centeno, A. Pesquera, A. Zurutuza, H. de Riedmatten, P. Goldner, F. J. Garcia de Abajo, P. Jarillo-Herrero, and F. H. L. Koppens, Electrical control of optical emitter relaxation pathways enabled by graphene, Nat. Phys. **11**, 281 (2015).

[14] B. Julsgaard, A. Walther, S. Kröll, and L. Rippe, Understanding laser stabilization using spectral hole burning, Opt. Express **15**, 11444 (2007).

[15] M. J. Thorpe, L. Rippe, T. M. Fortier, M. S. Kirchner, and T. Rosenband, Frequency stabilization to 6×10^{-16} via spectral-hole burning, Nat. Photonics **5**, 688 (2011).

[16] O. Gobron, K. Jung, N. Galland, K. Predehl, R. Letargat, A. Ferrier, P. Goldner, S. Seidelin, and Y. Le Coq, Dispersive heterodyne probing method for laser frequency stabilization based on spectral hole burning in rare-earth doped crystals, Opt. Express **25**, 15539 (2017).

[17] N. Galland, N. Lučić, S. Zhang, H. Alvarez-Martinez, R. Le Targat, A. Ferrier, P. Goldner, B. Fang, S. Seidelin, and Y. Le Coq, Double-heterodyne probing for ultra-stable laser based spectral hole burning in a rare-earth doped crystals, Opt. Lett. **45**, 1930 (2020).

[18] M. Aspelmeyer, P. Meystre, and K. Schwab, Quantum optomechanics, Phys. Today **65**, 29 (2012).

[19] I. Yeo, P.-L. de Assis, A. Gloppe, E. Dupont-Ferrier, P. Verlot, N. S. Malik, E. Dupuy, J. Claudon, J.-M. Gérard, A. Auffèves, G. Nogues, S. Seidelin, J. Poizat, O. Arcizet, and M. Richard, Strain-mediated coupling in a quantum dot-mechanical oscillator hybrid system, Nat. Nanotechnol. **9**, 106 (2014).

[20] J. Teissier, A. Barfuss, P. Appel, E. Neu, and P. Maletinsky, Strain Coupling of a Nitrogen-Vacancy Center Spin to a Diamond Mechanical Oscillator, Phys. Rev. Lett. **113**, 020503 (2014).

[21] P. Ovartchaiyapong, K. W. Lee, B. A. Myers, and A. C. Bleszynski Jayich, Dynamic strain-mediated coupling of a single diamond spin to a mechanical resonator, Nat. Commun. **5**, 4429 (2014).

[22] E. R. MacQuarrie, M. Otten, S. K. Gray, and G. D. Fuchs, Cooling a mechanical resonator with nitrogen-vacancy centres using a room temperature excited state spin-strain interaction, Nat. Commun. **8**, 14358 (2017).

[23] K. Mølmer, Y. Le Coq, and S. Seidelin, Dispersive coupling between light and a rare-earth-ion-doped mechanical resonator, Phys. Rev. A **94**, 053804 (2016).

[24] S. Seidelin, Y. Le Coq, and K. Mølmer, Rapid cooling of a strain-coupled oscillator by an optical phase-shift measurement, Phys. Rev. A **100**, 013828 (2019).

[25] R. W. Equall, Y. Sun, R. L. Cone, and R. M. Macfarlane, Ultraslow Optical Dephasing in Eu^{3+}:Y_2SiO_5, Phys. Rev. Lett. **72**, 2179 (1994).

[26] R. Oswald, M. G. Hansen, E. Wiens, A. Y. Nevsky, and S. Schiller, Characteristics of long-lived persistent spectral holes in Eu^{3+}:Y_2SiO_5 at 1.2 K, Phys. Rev. A **98**, 062516 (2018).

[27] F. Könz, Y. Sun, C. W. Thiel, R. L. Cone, R. W. Equall, R. L. Hutcheson, and R. M. Macfarlane, Temperature and concentration dependence of optical dephasing, spectral-hole

lifetime, and anisotropic absorption in Eu^{3+}:Y_2SiO_5, Phys. Rev. B **68**, 085109 (2003).

[28] G. Santarelli, A. Clairon, S. N. Lea, and G. M. Tino, Heterodyne optical phase-locking of extended-cavity semiconductor lasers at 9 GHz, Opt. Commun. **104**, 339 (1994).

[29] A. Ferrier, B. Tumino, and P. Goldner, Variations in the oscillator strength of the $^7F_0 \rightarrow {}^5D_0$ transition in single crystals, J. Lumin. **170**, 406 (2016).

[30] P. Jobez, N. Timoney, C. Laplane, J. Etesse, A. Ferrier, P. Goldner, N. Gisin, and M. Afzelius, Towards highly multimode optical quantum memory for quantum repeaters, Phys. Rev. A **93**, 032327 (2016).

[31] M. J. Thorpe, D. R. Leibrandt, and T. Rosenband, Shifts of optical frequency references based on spectral-hole burning in Eu^{3+}:Y_2SiO_5, New J. Phys. **15**, 033006 (2013).

[32] R. M. Macfarlane, A. Arcangeli, A. Ferrier, and P. Goldner, Optical Measurement of the Effect of Electric Fields on the Nuclear Spin Coherence of Rare-Earth Ions in Solids, Phys. Rev. Lett. **113**, 157603 (2014).

[33] Qian Li Yupan Bao, Axel Thuresson, Adam N. Nilsson, Lars Rippe, and Stefan Kröll, Slow-light-based optical frequency shifter, Phys. Rev. A **93**, 043832 (2016).

[34] R. J. Reeves and R. M. Macfarlane, Measurement of the effect of uniaxial stress on the spectrum of CaF_2:Pr^{3+}:D^- using spectral hole burning, Phys. Rev. B **39**, 5771 (1989).

[35] A. Louchet-Chauvet, R. Ahlefeldt, and T. Chanelière, Piezospectroscopic measurement of high-frequency vibrations in a pulse-tube cryostat, Rev. Sci. Instrum. **90**, 034901 (2019).

[36] G. Davies and M. F. Hamer, Optical studies of the 1.945 eV vibronic band in diamond, Proc. R. Soc. A **348**, 285 (1976).

[37] S. Meesala, Y.-I. Sohn, B. Pingault, L. Shao, H. A. Atikian, J. Holzgrafe, M. Göndogan, C. Stavrakas, A. Sipahigil, C. Chia, R. Evans, M. J. Burek, M. Zhang, L. Wu, J. L. Pacheco, J. Abraham, E. Bielejec, M. D. Lukin, M. Atatüre, and M. Loncar, Strain engineering of the silicon-vacancy center in diamond, Phys. Rev. B **97**, 205444 (2018).

[38] Ph. Tamarat, T. Gaebel, J. R. Rabeau, M. Khan, A. D. Greentree, H. Wilson, L. C. L. Hollenberg, S. Prawer, P. Hemmer, F. Jelezko, and J. Wrachtrup, Stark Shift Control of Single Optical Centers in Diamond, Phys. Rev. Lett. **97**, 083002 (2006).

[39] R. E. Evans, A. Sipahigil, D. D. Sukachev, A. S. Zibrov, and M. D. Lukin, Narrow-Linewidth Homogeneous Optical Emitters in Diamond Nanostructures via Silicon Ion Implantation, Phys. Rev. Appl. **5**, 044010 (2016).

[40] Z. Sun, J. Wang, M. Li, and Y. Zhou, Mechanical properties and damage tolerance of Y_2SiO_5, J. Eur. Ceram. Soc. **28**, 2895 (2008).

[41] J. Millo, D. V. Magalhaes, C. Mandache, Y. Le Coq, E. M. L. English, P. G. Westergaard, J. Lodewyck, S. Bize, P. Lemonde, and G. Santarelli, Ultrastable lasers based on vibration insensitive cavities, Phys. Rev. A **79**, 053829 (2009).

[42] S. Webster and P. Gill, Force-insensitive optical cavity, Opt. Lett. **36**, 3572 (2011).

[43] D. R. Leibrandt, J. C. Bergquist, and T. Rosenband, Cavity-stabilized laser with acceleration sensitivity below $10^{-12}g^{-1}$, Phys. Rev. A **87**, 023829 (2013).